



ARTICLE OPEN



The critical role of hot carrier cooling in optically excited structural transitions

Wen-Hao Liu^{1,2}, Jun-Wei Luo^{1,2,3} , Shu-Shen Li^{1,2,3} and Lin-Wang Wang⁴ 

The hot carrier cooling occurs in most photoexcitation-induced phase transitions (PIPTs), but its role has often been neglected in many theoretical simulations as well as in proposed mechanisms. Here, by including the previously ignored hot carrier cooling in real-time time-dependent density functional theory (rt-TDDFT) simulations, we investigated the role of hot carrier cooling in PIPTs. Taking IrTe₂ as an example, we reveal that the cooling of hot electrons from the higher energy levels of spatially extended states to the lower energy levels of the localized Ir–Ir dimer antibonding states strengthens remarkably the atomic driving forces and enhances atomic kinetic energy. These two factors combine to dissolve the Ir–Ir dimers on a timescale near the limit of atomic motions, thus initiating a deterministic kinetic phase transition. We further demonstrate that the subsequent cooling induces nonradiative recombination of photoexcited electrons and holes, leading to the ultrafast recovery of the Ir–Ir dimers observed experimentally. These findings provide a complete picture of the atomic dynamics in optically excited structural phase transitions.

npj Computational Materials (2021)7:117; <https://doi.org/10.1038/s41524-021-00582-w>

INTRODUCTION

The photoinduced phase transitions (PIPTs) have become an appealing approach exploring ultrafast change and manipulation of material properties owing to the recent advances in ultrafast time-resolved diffraction techniques, combining ultrafast temporal manipulation with atomic-scale spatial resolution^{1–22}. The optical excitation induces a nonequilibrium occupation of excited electronic states, which could lead to periodic lattice distortions (PLDs), expose the transient metastable states^{23,24}, or yield a controllable phase transition to the desired phase for practical applications^{5,9,10,21}. By means of photoexcitation, ultrafast phase transitions have been realized in quasi-one-dimensional (1D)^{5,6,10,16,17}, two-dimensional (2D)^{3,7,15,20,22}, and three-dimensional (3D)^{9,12,18,19,21} systems. One commonly used picture to explain the phase transition is the following: the photoexcited occupation of higher electronic states modifies the energy landscape substantially so that the original metastable phase becomes now a lower energy stable phase than the original ground state phase, causing the phase transition dynamically along the potential energy surfaces (PESs)^{5,7,9,25}. An alternative, yet related, picture is that the transient change in the PESs results in a non-thermal excitation of soft phonon modes, which leads to a critically damped nuclear motion following these soft phonon modes to the end phase of the PIPT^{5,25}. Our previous work²⁶ has also pointed out that the atomic forces for driving the PIPT in IrTe₂ arising from occupation of the Ir–Ir dimer antibonding (bonding) states by optically excited electrons (holes)²⁶. All these proposed explanations consider the photoexcited carriers as the cause for the change of PESs or the generation of additional atomic driving forces but disregard completely the phenomena of their relaxation to lower energy levels that occurred within the first hundred femtoseconds after photoexcitation.

IrTe₂ as a special quasi-2D layered transition-metal ditellurides is different from charge density wave (CDW) materials with the CDW gap^{27,28}. IrTe₂ both preserves its metallic properties in the low-

temperature (LT) phase with Ir–Ir dimerized $q = (1/5, 0, 1/5)$ lattice modulation, and in the high-temperature (HT) phase with the high symmetry^{27,28}. It is an interesting process to study the phase transition between the LT phase and HT phase in IrTe₂, but the mechanism of IrTe₂ phase transition is still under debate²⁸. In some recent experiments, the ultrafast PIPTs from LT-to-HT have been measured^{7,8}. Evidence has accumulated that hot carrier cooling may play an essential role in photoinduced ultrafast structural phase transitions in IrTe₂^{7,8}. For instance, Ideta et al. attributed the observed ultrafast recovery of Ir–Ir dimers following their dissolution to carrier recombination⁷. Monney et al. postulated that partial PIPT is driven by a transient increase of the lattice temperature following the hot carrier cooling in picoseconds⁸. We have also demonstrated that one can control the structural phase transitions by selectively exciting photocarriers into designated excited electronic states²⁶. The hot carrier cooling will undoubtedly alter the carrier's occupation to the excited states, thus changing the atomic driving forces. Besides, there are many possible effects in a PIPT, including electron–electron and electron–phonon interactions and thermal fluctuations. The lack of real-space atomic snapshots and the inability to turn on and off physical effects (e.g., electron–electron and electron–phonon interactions) experimentally renders it challenging to disentangle these interweaving physical effects relying on experimental measurements alone. Here, by including the previously ignored hot carrier cooling effect, we have advanced the real-time time-dependent density functional theory (rt-TDDFT) simulations to study the dynamical processes of PIPT.

In contrast, most current rt-TDDFT simulations can only describe the excited systems' immediate dynamics following the photoexcitation since they cannot describe the hot carrier cooling effect. Furthermore, in many simulations, optically excited electrons are mimicked by manually taking electrons from the top of the valence band and placed at the bottom of the conduction band, or thermally distributed using a very high temperature^{5,9,10,25,29,30}.

¹State Key Laboratory of Superlattices and Microstructures, Institute of Semiconductors, Chinese Academy of Sciences, Beijing, China. ²Center of Materials Science and Optoelectronics Engineering, University of Chinese Academy of Sciences, Beijing, China. ³Beijing Academy of Quantum Information Sciences, Beijing, China. ⁴Materials Science Division, Lawrence Berkeley National Laboratory, Berkeley, CA, USA. ✉email: jwluo@semi.ac.cn; lwwang@lbl.gov

Such simulations may provide a qualitative picture for PIPT, but it is unfeasible to reproduce the transition times behavior observed in the experiments accurately. An improvement has been made in some recent *rt*-TDDFT simulations using a Gaussian-envelope laser pulse to represent the actual laser light^{24,26,31}. But the use of Ehrenfest dynamics in the *rt*-TDDFT is unlikely to describe the carrier cooling correctly since it lacks the detailed balance. As a matter of fact, the Ehrenfest dynamics tend to overheat the electronic subsystem. In this work, to include the hot carrier cooling effect, we have improved our *rt*-TDDFT algorithm by including a Boltzmann factor³², which can restore the detailed balance between various electronic state transitions and hence treat the carrier cooling properly.

Figure 1 shows that after including the hot carrier cooling effect, the TDDFT simulation can precisely reproduce the experimentally measured femtosecond electron diffraction (FED) curve responsible for the complex phase transitions of IrTe₂ (including dissolution and recovery of Ir–Ir dimers) following photoexcitation. More specifically, the inclusion of the hot carrier cooling process in the state-of-the-art *rt*-TDDFT simulation significantly accelerates the phase transition within 300 fs compared to the usual *rt*-TDDFT simulations, which display no transition throughout the 1.2 ps simulation time. We will also explicitly illustrate that Ir–Ir dimers' ultrafast recovery following their dissolutions is caused by electrons' continuous cooling passing through the Fermi level towards nonradiative recombination with photoexcited holes. These results demonstrate that hot carrier cooling plays a vital role in the photoexcitation-induced structural phase transition.

RESULTS AND DISCUSSION

Photoinduced occupations of Ir–Ir dimerized antibonding states

To reveal the mechanism underlying the hot carrier cooling, we first examine the situation neglecting the hot carrier cooling process. More specifically, a straightforward *rt*-TDDFT simulation is carried out for the IrTe₂ system irradiated by a femtosecond laser pulse (central wavelength 400 nm, pulse duration 120 fs) with its amplitude tuned so that 3% of valence electrons is optically excited from the valence band to the conduction band (same as in experiments⁷). Figure 2a shows that immediately following the photoexcitation, only 40% of the empty Ir–Ir dimers' antibonding states are filled, and the rest of the photoexcited electrons occupy the higher energy states. In our previous work, we have demonstrated that the excited electrons occupying such higher energy states tend to suppress the LT-to-HT phase transition²⁶. We then proceed with the atomic dynamics by performing the *rt*-TDDFT simulation without including the Boltzmann factor as usual. As expected, no significant energy transfer occurs from photoexcited electrons to the lattice, and the lattice temperature remains around 200 K throughout the simulation. The top panel in Fig. 1b shows that, within the 1.2 ps simulation time, it is unlikely that the Ir–Ir dimers will undergo dissolution to achieve the LT-to-HT phase transition, which is quantified by the increase of Ir–Ir dimer bond length from 3.1 to 3.9 Å. One reason is that the photoelectrons fill only 40% of the Ir–Ir dimer's antibonding states, which is impossible to produce a strong enough atomic force to drive the phase transition.

Role of hot carrier cooling in photoinduced phase transition

In reality, hot carriers tend to relax to lower energy electronic states and give the released energy to the lattice through electron–phonon interaction^{1–3,11–15}. This transfer of energy also heats the lattice subsystem. To explore the hot carrier cooling effect, we carry out the *rt*-TDDFT simulation again but by adding a particular Boltzmann factor in the algorithm³². Figure 2b shows the dynamic evolution of excited electrons and holes following

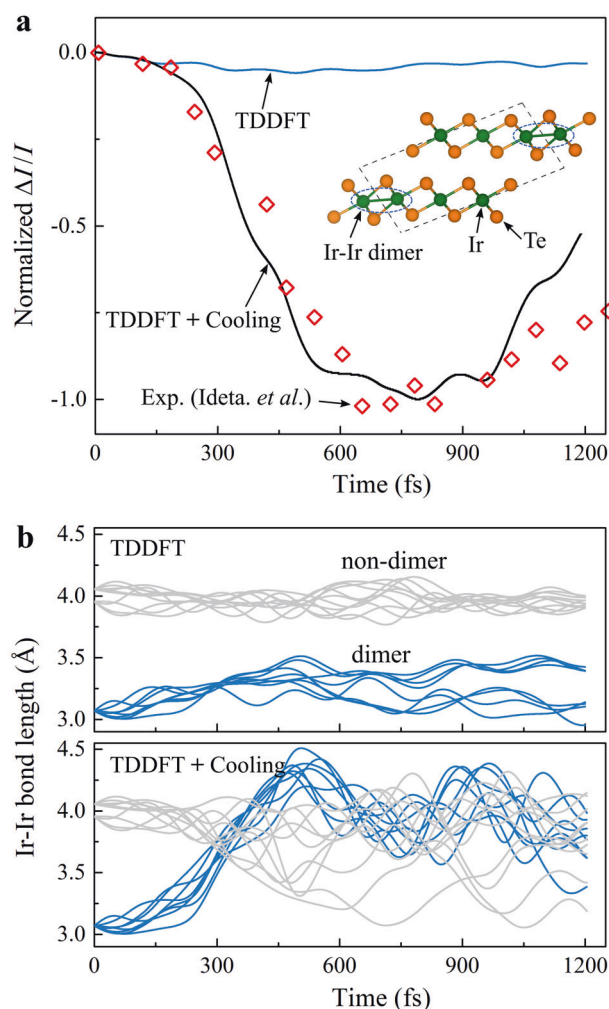


Fig. 1 Evolution of diffraction intensity and bond length. **a** Simulated PLD diffraction intensity $I(t)$ is obtained through the Debye–Waller formula^{40–42}, $I(t) = \exp[-Q^2 \langle u^2(t) \rangle / 3]$, where Q is the magnitude of the reciprocal lattice vector for the reflection probed, and $u^2(t)$ is average mean-square atomic displacements, as shown in Supplementary Fig. 1. Red diamonds show relative diffracted intensity changes ($\Delta I/I$) measured by FED experiments⁷. Note that the zero-point time in the experiment is far less than 0 at $t = 0$ fs. We reinstall the experimental data at $t = -380$ fs in ref. ⁷ as zero-point time in our work, giving a maximum value of the diffracted intensity at $t = 0$ fs. Blue and black lines represent the photoinduced lattice dynamics without and with the carrier cooling effect, respectively. The inset shows the LT phase with Ir–Ir dimerized $q = (1/5, 0, 1/5)$ lattice modulation^{27,28,43}. The black dashed box represents the unit cell. **b** The top (bottom) panel shows the evolution of eight-pair Ir–Ir dimers (blue lines) and ten non-dimerized Ir–Ir pairs (gray lines) in the TDDFT simulation without (with) the carrier cooling.

photoexcitation. It is necessary to evaluate the dynamic filling of the Ir–Ir dimers' antibonding states by electrons considering their occupation responsible for the atomic force driving the structural phase transition²⁶. To quantify it, here, we define n_{dimer} as the integration of the time-dependent (due to hot carrier cooling) electronic occupation of these states (located about 0.3–1.0 eV above the Fermi level as indicated in Fig. 2): $n_{\text{dimer}} = \int_{0.3}^{1.0} \rho_{\text{dimer}}(E, t) dE$. Figure 3a shows the development of n_{dimer} : it grows at first 120 fs from zero to a saturation value (120 fs) as a result of pulse laser photoexcitation, and then declines slightly from 120–150 fs, which indicates the emerging of

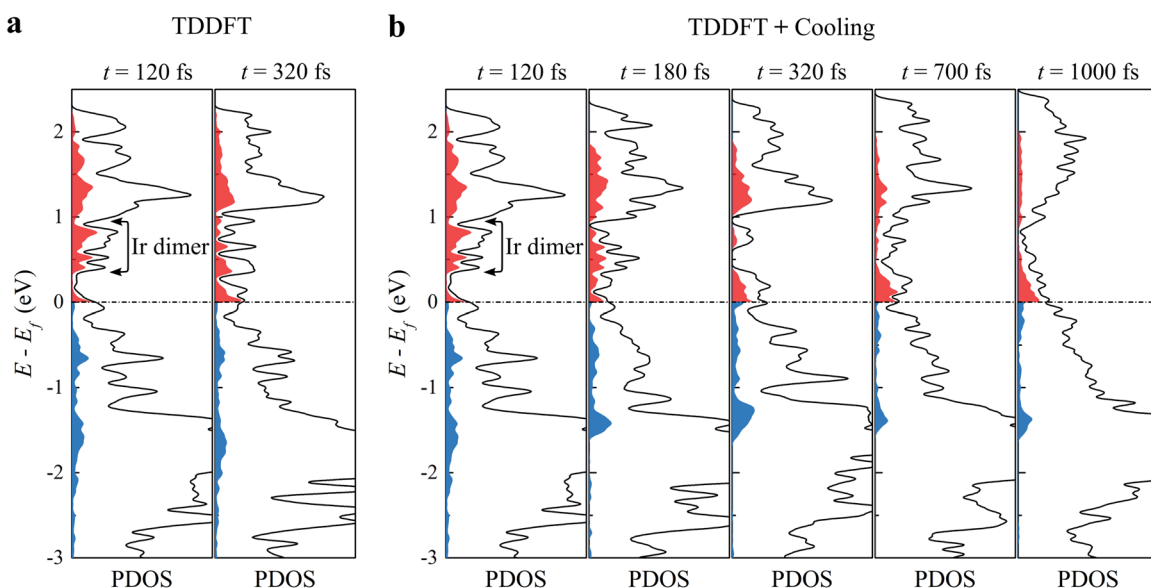


Fig. 2 Evolution of excited carriers. Partial density of states (PDOS) of eight-pair Ir–Ir dimers from TDDFT simulation without carrier cooling (**a**) and TDDFT simulation with carrier cooling (**b**). Red (blue) shaded areas represent 3% electronic occupations (hole occupations) where 40% Ir–Ir-dimerized antibonding states are occupied by photoexcited electrons at $t = 120$ fs.

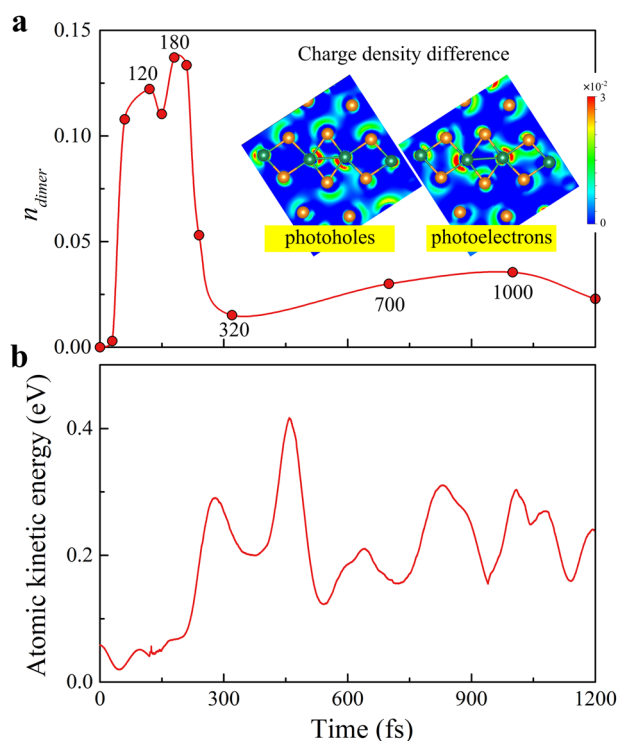


Fig. 3 Ir–Ir dimer antibonding occupations and kinetic energy. **a** Evolution of the electronic occupations on Ir–Ir dimerized antibonding states ($d_{xz} + d_{yz}$) within 0.3–1.0 eV above the Fermi level (see Supplementary Fig. 3). The inset shows the real-space charge density difference in the (11 $\bar{1}$) plane between the snapshots at 200 and 120 fs. **b** The averaged atomic kinetic energy of Ir–Ir dimers as a function of time.

hot carrier cooling process. Such decline is due to a net loss of excited electrons in the Ir–Ir dimers. The excited electrons belonging to them relax to lower energy states of other atoms but get fewer electrons from higher energy states. Figure 3b shows that, during the period, the atomic kinetic energy of the

Ir–Ir dimers stays at a low level, indicating the electron–electron interaction rather than phonon-assisted process dominates the carrier cooling. During this period, the Ir–Ir dimers’ bond length exhibits an invisible change (Fig. 1b).

The situation changes dramatically after 150 fs. Figure 2a shows that the photoexcited hot electrons begin to relax from higher energy levels to lower energy levels. The relaxation of hot carriers is also evidenced by the increase (a bump) in the electronic occupation of the Ir–Ir dimers’ antibonding states n_{dimer} from 150 to 210 fs, as shown in Fig. 3a. It is accompanied by an increase in the Ir–Ir dimer kinetic energy (Fig. 3b), manifesting the energy transfer of hot carrier cooling to the lattice subsystem. Thus, the phonon-assisted process is predominated in hot carrier cooling. The charge density difference between the snapshots at 200 and 120 fs (inset in Fig. 3a) displays that the photoexcited holes tend to localize at the Ir–Ir dimers’ bond center, and electrons prefer to stay at the two ends of the Ir–Ir dimers. Such localization due to hot carrier cooling manifests the characters of Ir–Ir dimers’ bonding and antibonding states, respectively. It strengthens remarkably the atomic forces for dissolution of the Ir–Ir dimers. The rapid increase of the atomic kinetic energy in the Ir–Ir dimers (Fig. 3b) should also speed up the Ir–Ir dimers’ dissolution by supplying enough energy to overcome any barriers. These two factors combined together render the Ir–Ir dimers undergoing an ultrafast dissociation at about 300 fs, as indicated in the bottom panel in Fig. 1b. Figure 2b and Supplementary Fig. 3 show that the Ir–Ir dimers’ dissolution is along with vanishing the peaks of the Ir–Ir dimers’ antibonding d -orbital states in DOS at 300 fs. From the time at which the lattice starts to be heating up by hot carrier cooling (at 150 fs) to the time at which the phase transition is completed (at 300 fs), the time for Ir motion is less than half of the vibrational period of the LO phonon (~ 1.2 THz) of IrTe₂²⁶. Such ultrafast phase transition induced by hot carrier cooling rules out the mechanisms based on unperturbed lattice mode³³. In the unperturbed coherent lattice mode, the timescale of phase transition is the half-cycle oscillation of the coherent amplitude mode^{33,34}.

To verify the effect of the increase in the atomic kinetic energy of Ir dimers unambiguously, we re-do our simulation in the NVT ensemble during carrier cooling. In contrast to the above-adopted NVE ensemble, which considers the energy transfer from hot

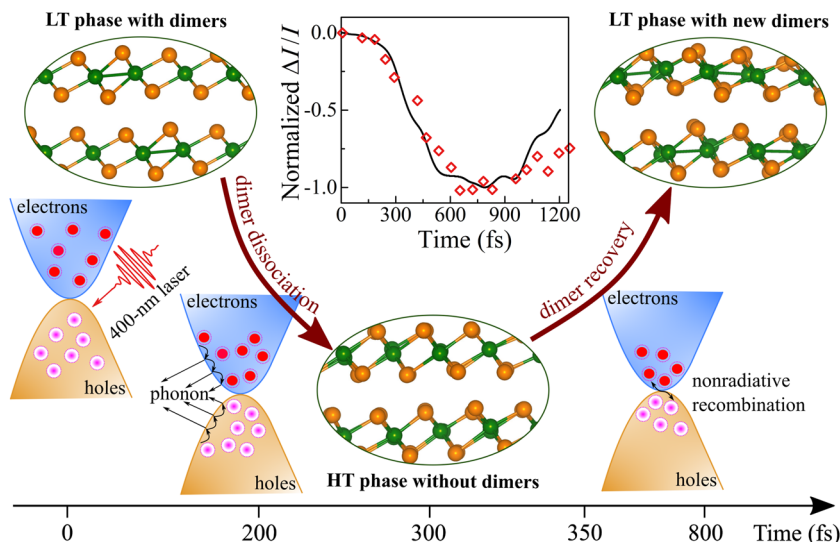


Fig. 4 Photoinduced ultrafast dynamics with hot carrier cooling strongly coupled to the lattice. Laser-induced the electron–hole pairs within 120 fs; Hot carrier cooling from high-energy levels to low-energy levels; The recombination of electron–hole pairs; Structural dynamics following photoexcitation are driven by electron–phonon couplings.

carrier cooling to the kinetic energy in the transition degree of freedom³², in the NVT the lattice kinetic energy is kept constant for a given initial temperature to mimic a situation for heat dissipates quickly. Supplementary Fig. 2 shows that in this case, the increase in the occupation of the Ir–Ir dimers’ antibonding states strengthens the atomic driving forces following hot carrier cooling. However, the Ir–Ir dimers are unable to be dissociated due exclusively to the absence in the enhancement of the Ir–Ir dimer kinetic energy. Considering the lattice can only oscillate half of its vibrational period during hot carrier cooling, as discussed above, it is difficult to claim that its kinetic energy will be dissipated out as heat during that time. Thus, we believe the NVE simulation is more close to reality. We subsequently conclude that the hot carrier cooling inducing the increase of Ir dimer kinetic energy plays a vital role in the structural phase transition.

Carrier recombination to drive recovery of phase transition

Furthermore, the enhanced atomic forces drive the Ir–Ir dimers’ dissolution to have a deterministic and coherent manner without exhibiting a significant random fluctuation. Figure 1 shows that the system completes the LT-to-HT phase transition at 300 fs; however, the maximum change in the diffraction intensities is delayed and achieved later at 750 fs as observed in both experimental measurements⁷ and our theoretical simulation. Such delay has also been detected in PIPT of the CDW material 1T-TaS₂¹ and is considered as the combination of the displacive excitation of highly correlated atomic motions and phonon-induced disorder contribution to the suppression of diffraction intensity.

After reaching the minimum at around 750 fs, Fig. 1a shows that the diffraction intensity change begins to rise, which was postulated as the recovery of the Ir–Ir dimerization⁷. Here, we confirm this postulation theoretically and reveal the underlying mechanism. The difference from semiconductors, IrTe₂ lacks a bandgap. Thus, the cooling of the optically excited electrons is unlikely to end at the bottom of the conduction band due to the phonon bottleneck as in semiconductors. Instead, excited electrons cool down continuously, passing the Fermi energy to finally fill the holes in the valence bands, making nonradiative recombination of electrons and holes without photons’ emission. Figure 3b shows that the number of excited electrons starts to drop rapidly at 210 fs, indicating the electron–hole nonradiative recombination that releases the atomic driving forces exerting on

the Ir–Ir dimers. At this moment, these Ir atoms have been accelerated to high speeds. These residual speeds drive them towards the nearest neighbor of non-dimerized Ir atoms to form dimers (Fig. 4). Interestingly, these dimers are formed even though their lattice temperature ($T \sim 900$ K) is well above the critical temperature $T_S = 280$ K of thermal-induced phase transition²⁸. It shows, once again, the phase transition is a coherent kinetic process, not a thermodynamic random process. Although the atomic kinetic energy is important (as demonstrated in the NVE simulation) in a photoinduced phase transition, its role is unlikely as in the thermodynamic phase transition but a kinetic movement to overcome barriers towards breaking the old dimer and forming the dimers. Accompanying the Ir–Ir dimerization, the vanished antibonding states of Ir–Ir dimers above the Fermi level re-appear in the PDOS (see Supplementary Fig. 3). Therefore, we have developed a microscopic explanation for the observed ultrafast recovery of PLD in experiments⁷. We also record the structural phase change evolution dynamics following photoexcitation in a movie (given in Supplementary Movie). In short, we reproduced the experimentally measured change of the diffraction intensity following the photoexcitation, in both magnitude and time scale. All this is only possible after we take into account the carrier cooling effect.

Our excellent agreement with the experiment also supports a fast sub-picosecond energy transfer from electron to phonon. It contrasts with a common perception that the electron to phonon energy transfers is a slow process in several ps, as judged by the observed electron–phonon equilibration time (several ps)^{35,36}. We believe this long electron–phonon equilibration time is mainly due to the equilibration process of lattice thermal motions following the initial coherent motions with atomic kinetic energy obtained from the carrier cooling. After the lattice vibration reaches equilibrium, the system will finally transfer from the new PLD structure to the HT phase due to its high lattice temperature ($T \sim 900$ K, which is well above the critical temperature $T_S = 280$ K). We indeed notice that a much slower phase transition following photoexcitation has also been reported experimentally in IrTe₂⁸. However, this should be distinguished from the sub-picosecond diffraction measurement shown in Fig. 1a. To examine the temperature-induced structural phase transition, we utilize a Born–Oppenheimer MD (BOMD) to simulate the lattice dynamics of the system in the ground state at lattice temperature $T \approx 1000$ K but without photoexcitation (see Supplementary Fig. 5). We

indeed find that the Ir–Ir dimers undergo a dissolution at about 6.5 ps, a time scale nearly one order of magnitude slower than the PIPT. In this case, high lattice temperature is the only aspect responsible for this structural phase transition.

In summary, we have unraveled the critical role of the hot carrier cooling in the photoexcitation-induced structural phase transition by performing rt-TDDFT simulations including a Boltzmann factor to model the hot carrier cooling process. As summarized in Fig. 4, if the pump laser pulse's photon energy is much larger, the photoexcited electrons and holes have a widespread distribution in energy inside the conduction and valence bands. The widespread distribution of photoexcited carriers will not exert a sufficiently large atomic force to dissociate the Ir–Ir dimers. On the other hand, the hot carrier cooling will have two major effects, which help the Ir–Ir dimer dissolution: first, there will be more occupation of the Ir–Ir dimer antibonding state, which enhances the atomic force to dissociate the dimer; second, the atoms of the Ir–Ir dimers will gain considerable coherent kinetic energies, which can help them to overcome any barrier during the dimer breaking process. In a combination of these two factors, the hot carrier cooling yields a phase transition curve in excellent agreement with the experimentally observed time-resolved diffraction data. We further show that the transition is deterministic and coherent. The coherent kinetic energy induces the formation of the Ir–Ir dimers (at different locations from the initial ones), contributing to the experimentally observed sub-picosecond recovery of the LT phase. On the other hand, for a thermal equilibrium system to induce phase transition due to its high-temperature effect, it can take about 6.5 ps, ten times longer than the fast coherent phase transition caused by hot carrier cooling. We believe our current understanding presents an insight into photoexcitation-induced ultrafast phase transitions. It is likely also applicable to other ultrafast phase transitions for systems like vanadium dimers in VO_2 ^{9,18} and CDW material 1T-TaS₂¹, 1T-TiSe₂^{2,14}, and 1T-LaTe₃^{13,15}.

METHODS

Real-time TDDFT

We carry out the rt-TDDFT simulations³⁷ based on the norm-conserving pseudopotentials (NCP)³⁸ and Perdew–Burke–Ernzerhof (PBE) functional within density functional theory (DFT) framework with a plane wave nonlocal pseudopotential Hamiltonian, which is implemented in the code PWmat³⁹. The wave functions were expanded on a plane-wave basis with an energy cutoff of 45 Ryd. In the rt-TDDFT simulation, we use a 128-atom supercell for IrTe₂ and the Γ point was used to sample the Brillouin zone. In this rt-TDDFT algorithm, the time-dependent wave functions, $\psi_i(t)$, are expanded by the adiabatic eigenstates, $\phi_l(t)$:

$$\psi_i(t) = \sum_l C_{il}(t)\phi_l(t) \quad (1)$$

and

$$H(t)\phi_l(t) \equiv \varepsilon_l(t)\phi_l(t) \quad (2)$$

Here, $H(t) \equiv H(t, R(t), \rho(t))$, $R(t)$ represents the nuclear positions, and $\rho(t)$ represents the charge density. By using Eq. (1), the evolution of the wave functions $\psi_i(t)$ is changed to the evolution of the coefficient $C_{il}(t)$. In Eq. (2), a linear-time-dependent Hamiltonian (LTDH) is applied to represent the time dependence of the Hamiltonian within a time step. Thus, we can obtain a much larger time step (0.1–0.2 fs) than the conventional real-time TDDFT (sub-attosecond), and the time step is set to 0.1 fs in our simulation.

To mimic the photoexcitation, we apply an external electric field to simulate a laser pulse with a Gaussian shape in our rt-TDDFT,

$$E(t) = E_0 \cos(\omega t) \exp[-(t - t_0)^2 / (2\sigma^2)] \quad (3)$$

where $E_0 = 0.2 \text{ V/\AA}$, $t_0 = 60 \text{ fs}$, $2\sigma = 25 \text{ fs}$ is the pulse width, and $\omega = 3.1 \text{ eV}$ is the photon energy⁷.

Boltzmann formula in rt-TDDFT

To depict hot carrier cooling, we utilize the Boltzmann formula in rt-TDDFT³². Boltzmann formula will depend on adiabatic state $\phi_l(t)$ in Eq. (1). After Boltzmann correlation ($e^{-t/\tau_{ij}}$, here, τ_{ij} is a decoherence time of 20 fs in the text. Note that, these conclusions do not sensitively depend on the choice of τ_{ij} as shown in Supplementary Fig. 4. The use of $\tau = 20 \text{ fs}$ is based on an estimation following a procedure described in SI), a change $\Delta C_{il}(t)$ is introduced in the coefficient $C_{il}(t)$, thus, the wave function is updated

$$\psi_i(t) = \sum_l (C_{il}(t) + \Delta C_{il}(t))\phi_l(t) \quad (4)$$

Compared with total energy (E_{tot1}) calculated in Eq. (1), the total energy (E_{tot2}) is indeed changed in Eq. (4). Based on the change of energy, we can obtain the increased kinetic energy which embodies the el–ph coupling effect. This energy will be added to the transition degree of freedom in the NVE ensemble. For a more detailed description of the Boltzmann factor formalism, we refer to it in ref. ³⁰. In the NVT ensemble with carrier cooling, the total kinetic energy of all the atoms is kept the same by a simple rescaling.

Born–Oppenheimer MD

A 128-atom supercell for IrTe₂ and the Γ point to sample the Brillouin zone are used in BOMD. After geometry optimization at static calculation, we use NVE ensemble: the lattice temperature always oscillates around the set temperature of 1000 K in Supplementary Fig. 5.

DATA AVAILABILITY

The data that support the findings of this study are available from the corresponding authors upon reasonable request.

CODE AVAILABILITY

The rt-TDDFT CODE has been integrated in the PWmat package. The PWmat software can also be accessed directly from <http://www.pwmat.com>.

Received: 21 March 2021; Accepted: 29 June 2021;

Published online: 22 July 2021

REFERENCES

- Eichberger, M. et al. Snapshots of cooperative atomic motions in the optical suppression of charge density waves. *Nature* **468**, 799–802 (2010).
- Rohwer, T. et al. Collapse of long-range charge order tracked by time-resolved photoemission at high momenta. *Nature* **471**, 490–493 (2011).
- Laulhe, C. et al. Ultrafast formation of a charge density wave state in 1T-TaS₂: observation at nanometer scales using time-resolved X-ray diffraction. *Phys. Rev. Lett.* **118**, 247401 (2017).
- Ishikawa, T. et al. Direct observation of collective modes coupled to molecular orbital-driven charge transfer. *Science* **350**, 1501–1505 (2015).
- Frigge, T. et al. Optically excited structural transition in atomic wires on surfaces at the quantum limit. *Nature* **544**, 207–211 (2017).
- Chávez-Cervantes, M., Krause, R., Aeschlimann, S. & Gierz, I. Band structure dynamics in indium wires. *Phys. Rev. B* **97**, 201401(R) (2018).
- Ideta, S. I. et al. Ultrafast dissolution and creation of bonds in IrTe₂ induced by photodoping. *Sci. Adv.* **4**, 3867 (2018).
- Monney, C. et al. Robustness of the charge-ordered phases in IrTe₂ against photoexcitation. *Phys. Rev. B* **97**, 075110 (2018).
- Wall, S. et al. Ultrafast disordering of vanadium dimers in photoexcited VO₂. *Science* **362**, 572–576 (2018).
- Nicholson, C. W. et al. Beyond the molecular movie: dynamics of bands and bonds during a photoinduced phase transition. *Science* **362**, 821–825 (2018).
- Okazaki, K. et al. Photo-induced semimetallic states realised in electron–hole coupled insulators. *Nat. Commun.* **9**, 4322 (2018).
- Tengdin, P. et al. Critical behavior within 20 fs drives the out-of-equilibrium laser-induced magnetic phase transition in nickel. *Sci. Adv.* **4**, 9744 (2018).
- Zong, A. et al. Evidence for topological defects in a photoinduced phase transition. *Nat. Phys.* **15**, 27–31 (2018).
- Hedayat, H. et al. Excitonic and lattice contributions to the charge density wave in 1T–TiSe₂ revealed by a phonon bottleneck. *Phys. Rev. Res.* **1**, 023029 (2019).

15. Kogar, A. et al. Light-induced charge density wave in LaTe_3 . *Nat. Phys.* **16**, 159–163 (2019).
16. Chavez-Cervantes, M. et al. Charge density wave melting in one-dimensional wires with femtosecond subgap excitation. *Phys. Rev. Lett.* **123**, 036405 (2019).
17. Nicholson, C. W. et al. Excited-state band mapping and momentum-resolved ultrafast population dynamics in In/Si(111) nanowires investigated with XUV-based time- and angle-resolved photoemission spectroscopy. *Phys. Rev. B* **99**, 155107 (2019).
18. Otto, M. R. et al. How optical excitation controls the structure and properties of vanadium dioxide. *Proc. Natl Acad. Sci. USA* **116**, 450–455 (2019).
19. Rana, R. et al. Nonthermal nature of photoinduced insulator-to-metal transition in NbO_2 . *Phys. Rev. B* **99**, 041102(R) (2019).
20. Sie, E. J. et al. An ultrafast symmetry switch in a Weyl semimetal. *Nature* **565**, 61–66 (2019).
21. Vidal, F. et al. Ultrafast structural dynamics along the beta-gamma phase transition path in MnAs . *Phys. Rev. Lett.* **122**, 145702 (2019).
22. Zhang, M. Y. et al. Light-Induced subpicosecond lattice symmetry switch in MoTe_2 . *Phys. Rev. X* **9**, 021036 (2019).
23. Sun, K. et al. Hidden CDW states and insulator-to-metal transition after a pulsed femtosecond laser excitation in layered chalcogenide $1\text{T-TaS}_{2-x}\text{Se}_x$. *Sci. Adv.* **4**, 9660 (2018).
24. Zhang, J. et al. Photoexcitation induced quantum dynamics of charge density wave and emergence of a collective mode in 1T-TaS_2 . *Nano Lett.* **19**, 6027–6034 (2019).
25. Chen, N. K. et al. Directional forces by momentumless excitation and order-to-order transition in peierls-distorted solids: the case of GeTe . *Phys. Rev. Lett.* **120**, 185701 (2018).
26. Liu, W.-H., Luo, J.-W., Li, S.-S. & Wang, L.-W. Microscopic force driving the photoinduced ultrafast phase transition: Time-dependent density functional theory simulations of IrTe_2 . *Phys. Rev. B* **102**, 184308 (2020).
27. Pascut, G. L. et al. Dimerization-induced cross-layer quasi-two-dimensionality in metallic IrTe_2 . *Phys. Rev. Lett.* **112**, 086402 (2014).
28. Kim, K. et al. Origin of first-order-type electronic and structural transitions in IrTe_2 . *Phys. Rev. Lett.* **114**, 136401 (2015).
29. Chen, N.-K. et al. Optical subpicosecond nonvolatile switching and electron–phonon coupling in ferroelectric materials. *Phys. Rev. B* **102**, 184115 (2020).
30. Wang, X.-P. et al. Time-dependent density-functional theory molecular-dynamics study on amorphization of Sc-Sb-Te alloy under optical excitation. *npj Comput. Mater.* **6**, 31 (2020).
31. Lian, C., Zhang, S. J., Hu, S. Q., Guan, M. X. & Meng, S. Ultrafast charge ordering by self-amplified exciton–phonon dynamics in TiSe_2 . *Nat. Commun.* **11**, 43 (2020).
32. Wang, L. W. Natural orbital branching scheme for time-dependent density functional theory nonadiabatic simulations. *J. Phys. Chem. A* **124**, 9075–9087 (2020).
33. Sciaini, G. et al. Electronic acceleration of atomic motions and disordering in bismuth. *Nature* **458**, 56–59 (2009).
34. Fritz, D. M. et al. Ultrafast bond softening in bismuth: mapping a solid’s interatomic potential with X-rays. *Science* **315**, 633–636 (2007).
35. Rouse, A. et al. Non-thermal melting in semiconductors measured at femtosecond resolution. *Nature* **410**, 65–68 (2001).
36. Peng, B. et al. Sub-picosecond photo-induced displacive phase transition in two-dimensional MoTe_2 . *npj 2D Mater. Appl.* **4**, 14 (2020).
37. Wang, Z., Li, S. S. & Wang, L. W. Efficient real-time time-dependent density functional theory method and its application to a collision of an ion with a 2D material. *Phys. Rev. Lett.* **114**, 063004 (2015).
38. Hamann, D. R. Optimized norm-conserving Vanderbilt pseudopotentials. *Phys. Rev. B* **88**, 085117 (2013).
39. Jia, W. L. et al. The analysis of a plane wave pseudopotential density functional theory code on a GPU machine. *Comput. Phys. Commun.* **184**, 9–18 (2013).
40. Lindenberg, A. M. et al. Atomic-scale visualization of inertial dynamics. *Science* **308**, 392–395 (2005).
41. Harb, M. et al. Electronically driven structure changes of Si captured by femto-second electron diffraction. *Phys. Rev. Lett.* **100**, 155504 (2008).
42. VandenBussche, E. J. & Flannigan, D. J. Sources of error in Debye–Waller-effect measurements relevant to studies of photoinduced structural dynamics. *Ultra-microscopy* **196**, 111–120 (2019).
43. Toriyama, T. et al. Switching of conducting planes by partial dimer formation in IrTe_2 . *J. Phys. Soc. Jpn.* **83**, 033701 (2014).

ACKNOWLEDGEMENTS

The work in China was supported by the Key Research Program of Frontier Sciences, CAS under Grant No. ZDBS-LY-JSC019, the Strategic Priority Research Program of the Chinese Academy of Sciences under Grant No. XDB43020000, and the National Natural Science Foundation of China (NSFC) under Grant Nos. 11925407 and 61927901. L.-W.W. was supported by the Director, Office of Science (SC), Basic Energy Science (BES), Materials Science and Engineering Division (MSED), of the US Department of Energy (DOE) under Contract No. DE-AC02-05CH11231 through the Materials Theory program (KC2301).

AUTHOR CONTRIBUTIONS

W.-H.L. performed the TDDFT simulations and prepared the figures. J.-W.L. and L.-W.W. proposed the research project, established the project direction and conducted the analysis, discussion, and writing of the paper with input from W.-H.L. S.-S.L. provided the project infrastructure and supervised W.-H.L.’s study.

COMPETING INTERESTS

The authors declare no competing interests.

ADDITIONAL INFORMATION

Supplementary information The online version contains supplementary material available at <https://doi.org/10.1038/s41524-021-00582-w>.

Correspondence and requests for materials should be addressed to J.-W.L. or L.-W.W.

Reprints and permission information is available at <http://www.nature.com/reprints>

Publisher’s note Springer Nature remains neutral with regard to jurisdictional claims in published maps and institutional affiliations.



Open Access This article is licensed under a Creative Commons Attribution 4.0 International License, which permits use, sharing, adaptation, distribution and reproduction in any medium or format, as long as you give appropriate credit to the original author(s) and the source, provide a link to the Creative Commons license, and indicate if changes were made. The images or other third party material in this article are included in the article’s Creative Commons license, unless indicated otherwise in a credit line to the material. If material is not included in the article’s Creative Commons license and your intended use is not permitted by statutory regulation or exceeds the permitted use, you will need to obtain permission directly from the copyright holder. To view a copy of this license, visit <http://creativecommons.org/licenses/by/4.0/>.

© The Author(s) 2021